Research Article | Vol. 32, No. 10 / 6 May 2024 / Optics Express 18399
Optics EXPRESS

Long-wave infrared pulsed external-cavity QCL spectrometer using a hollow waveguide gas cell

DANIEL FRANCIS,* JANE HODGKINSON, AND RALPH P. TATAM

Engineering Photonics, Cranfield University, MK43 0AL, UK
*daniel.francis@cranfield.ac.uk

Abstract: A spectrometer built using an external cavity pulsed quantum cascade laser is described. The spectrometer has a tuning range from 10 – 13 μm (1,000 – 769 cm^{-1}) and is designed to target volatile organic compounds (VOCs) which often exhibit water-free molecular absorption within the region. The spectrometer utilizes a hollow silica waveguide gas cell which has an internal volume of a few millilitres, a fast response time (~1 s), and is advantageous when only low sample volumes, similar to the cell volume, are available. Propane is used as a test gas because it is easy to handle, and its spectral profile is comparable to VOCs of interest. Its absorption in the region is primarily within the ν_{21} band which spans from 10.55 – 11.16 μm (948 – 896 cm^{-1}). Spectral measurements at a range of concentrations show good linearity and an Allan deviation of absorbance values recorded over a 100-minute period indicates a minimum detectable absorbance of 3.5×10^{-5} at an integration time of 75 s.

Published by Optica Publishing Group under the terms of the Creative Commons Attribution 4.0 License. Further distribution of this work must maintain attribution to the author(s) and the published article's title, journal citation, and DOI.

1. Introduction

Quantification of the volatile organic compounds (VOCs) present in a range of biological matrices including breath, urine, blood, and faeces is of interest in medical diagnostics. Variation of the VOC profile has been associated with the biological processes of diseases including Parkinson's [1], gastro-intestinal diseases such as Crohn's disease and ulcerative colitis [2], and lung infections such as *pseudomonas aeruginosa* [3]. VOC quantification has been achieved through collection of the headspace gas of bodily fluids onto sorbent tubes, followed by thermal desorption for analysis using gas-chromatography mass-spectrometry (GC-MS) [2]. However, GC-MS can be complex and intensive, require skilled personnel to operate the equipment, and typically require sampling and storage of headspace gases before they can be analysed, making it less than ideal for point-of-care instrumentation.

Tuneable laser absorption spectroscopy (TLAS) [4] is a well-established technique for measuring gas concentrations and is known for its high degree of sensitivity and selectivity [5]. It has found use in numerous applications including environmental and industrial monitoring [6], medical diagnostics [7,8], security [9,10], and leak detection [11] amongst others. Identification and quantification of gaseous samples is achieved through detection of their spectral absorption features which are unique for each species. Absorption occurs across the electromagnetic spectrum and for many species spectral absorption is strongest in the mid-infrared from ~3 – 8 μm [12].

The development of quantum cascade (QC) [13] and interband cascade (IC) lasers [14] emitting at wavelengths from 3.5 – 19 μm [15] has driven significant improvement in quantitative spectroscopic measurement. Distributed feedback (DFB) QCLs offer narrowband emission with typical tuning ranges of several nanometres achieved through modulation of the injection current or temperature. These lasers are particularly suitable for gas species that have relatively small molecules since these have spectral absorption features that are narrower than the tuning range of the laser. This is manifested in the commercial availability of lasers with emissions

#521695 https://doi.org/10.1364/OE.521695
Journal © 2024 Received 1 Mar 2024; revised 10 Apr 2024; accepted 10 Apr 2024; published 3 May 2024

Optics EXPRESS

corresponding to the significant water-free absorptions of these molecules. For larger molecules, such as (VOCs), absorption spectra are more complex, and often contain features that are much wider than the tuning range of DFB QCLs. Whilst many VOC molecules exhibit absorption in the 5 – 8 μm region, these can be subject to interference from water absorption, however they also typically absorb in the long-wave infrared region from ~8 – 15 μm [16].

External-cavity QCLs (EC-QCLs) are an excellent option for spectroscopy of these larger molecules because they provide much wider tuning ranges than DFB lasers, reaching up to several micrometres. However, this comes at the cost of lower spectral resolution than DFB lasers. EC-QCLs usually rely on a diffraction grating, typically in either the Littrow or Littman configuration, to selectively reflect different wavelengths into the cavity to achieve these large tuning ranges [17]. The breadth of applications of EC-QCL spectroscopy is significant and diverse as is highlighted in Table 1, which summarizes some of the measurements made across the scientific community and includes the laser and wavelength ranges used and the gas cell configuration. Target analytes include proteins [18,19], explosives [20–22], and VOCs [23,24], as well as mixtures of smaller atmospheric species using a non-commercial laser with improved spectral resolution [25,26]. Most examples use commercially available sources from Daylight Solutions or Block Engineering that are either pulsed or continuous wave (CW). Whilst there are several examples of standoff detection, most experimenters use single or multi-pass gas cells. There is also interest in gas cells made of hollow waveguides which, because of their high pathlength to volume ratio, are ideal for low-volume samples. Recently, an alternative approach to VOC spectroscopy has been reported which utilizes Vernier-type QCLs [27]. These offer a unique compromise between DFB and EC QCLs, in that their achieved spectral resolution is close to that achieved using DFB lasers but with a larger spectral window (though less than with EC-QCLs). The Vernier QCL reported in [27] has a tuning range of ~330 nm centred at ~9.24 μm.

Low volume gas cells are desirable due to their rapid fill times and are advantageous when only small amounts of sample (~mls) are available. Gas cells formed from hollow waveguides and fibres have generated significant interest [28] and have been constructed from numerous materials including photonic crystal fibre (PCF) [29,30] and substrate integrated waveguides formed of two-part solid, e.g. aluminium, slabs with waveguide structures embedded [31]. Another frequently used material is hollow silica waveguide (HSW) [32,33]. This structure consists of a silica tube that is internally coated with silver using a wet chemistry technique. The silver is exposed to a halogen that converts some of the silver to a silver halide, the ratio of which determines the peak spectral reflectivity of the waveguide. The bore diameter of HSW typically varies from a few hundreds to about a thousand micrometres and this determines transmission, with larger bore waveguides experiencing reduced optical losses at the cost of reduced mechanical flexibility. Single mode transmission is achievable, and this depends on the launch parameters and waveguide coiling, as well as the operating wavelength and bore diameter [34,35]. Gas cells constructed using HSW are low volume, typically a few millilitres, though this is increased by any dead space introduced by gas input coupling that is added to the waveguide to form the cell. The diameter of HSW is not so narrow that prohibitively long fill times occur, as can be an issue with some PCF gas cells, indeed fast response times of the order of a second can be achieved with practical flow rates (up to 1 litre/min) [36]. Hollow waveguide gas cells have also been used with quartz enhanced photo-acoustic spectroscopy (QEPAS) [37,38] and recently light induced thermoelastic spectroscopy (LITES) [39,40].

This paper describes the development of a pulsed EC-QCL spectrometer which incorporates a HSW gas cell. The source has a spectral coverage of 10 – 13 μm and this is the first report of this combination operating at this wavelength range. The system is intended primarily for spectroscopy of VOCs however here measurements are presented using propane, which is a convenient and easy to handle test gas. Absorption of propane within the coverage of the

Optics EXPRESS

Table 1. Measurements made by various researchers using external-cavity quantum cascade laser spectroscopy. The wavelength range refers to the total spectral coverage of the source, as the experimental scan may be less in some cases. (RDX = research department explosive, VOC = volatile organic compound, DS = Daylight Solutions, PNNL = Pacific Northwest National Laboratory, BE = Block Engineering, CW = continuous wave, PW = pulsewidth, PCD = polycrystalline diamond, HSW = hollow silica waveguide).

Species	Source	Output	WL range (μm)[a]	Gas cell	Ref
Saliva enzymes	DS (MIRcat)	Pulsed (PW = 400 ns)	4.95 - 11.2 (4 QCLs)	PCD waveguide	[42]
Proteins	DS	Pulsed (PW = 500 ns)	5.78 - 6.39	Single pass	[18]
Proteins	DS (Hedgehog)	Pulsed (PW = 5 μs)	5.78 - 6.80	Single pass	[19]
Hydro carbons	DS (MIRcat-1400)	CW	6 - 11	Single pass	[43]
RDX	DS (MIRcat)	CW	6 - 11	Single pass	[20]
NO_2	DS (TLS-MHF)	CW	6.08 - 6.15	Multi-pass	[44]
RDX	DS (MIRcat)	Pulsed (PW = 500 ns)	6.13 - 12.5 (4 QCLs)	Standoff detection	[21]
Explosives	DS (UberTuner)	Pulsed (PW = 500 ns)	6.2 - 7.6	Multi-pass	[22]
Mixed inc. VOCs	PNNL custom laser	CW	6.73 - 7.78	HSW waveguide	[25]
Mixed VOCs	BE	Pulsed (PW < 350 ns)	6.96 - 8.85	Standoff detection	[23,24]
Iso-butane	BE (Laserscope)	Pulsed (PW = 48 ns)	7 - 12	Shock tube	[45]
Mixed inc. CH_4, SO_2	PNNL custom laser	CW	7.19 - 7.81	Multi-pass	[26]
Chlorides	DS	Pulsed (PW = 500 ns)	7.7 - 8.2	Hollow waveguide	[46]
N_2O_5	DS (CW-MHF)	CW	7.92 - 8.18	Multi-pass	[47]
Fluoro-carbons	PNNL custom laser	CW	7.94 - 8.77	Multi-pass	[48]
Multi inc. acetone	BE (Laserscope)	Pulsed (PW = 208 ns)	8.0 - 11.8	Multi-pass	[49,50]
Ethylene C_2H_4	DS (MIRcat)	CW	8.5 - 10.5, 10.5 - 11.7	Shock tube	[51]
Benzene/ toluene	DS (TLS-MHF)	CW	9.41 - 9.88	Multi-pass	[52]
Propane	*DS (MIRcat)*	*Pulsed (PW = 500 ns)*	*10 - 13*	*HSW waveguide*	[*This work*]

[a]Table ordered by lower wavelength in range

spectrometer is dominated by the ν_{21} band which is an A-type band arising from rotations within the methyl groups [41]. It is centred at 10.85 μm (922 cm^{-1}) and covers the range 10.55 – 11.16 μm (948 – 896 cm^{-1}). The propane absorption band is not particularly useful in itself since it is weaker than other, more prominent bands of the molecule, nevertheless it makes a useful test case in the spectral region in which we are interested.

One of the VOCs that is of particular interest is *p*-cresol (4-methyl phenol), as it has been identified as a biomarker for *clostridium-difficile* infection [53] and has a prominent, water-free absorption centred at approximately 12.2 μm (820 cm^{-1}) [54]. This absorption is also relatively

Optics EXPRESS

free from interference from other hydrocarbons and has a similar spectral width and complexity to the ν_{21} band of propane whilst being approximately 50 times stronger. Other volatile biomarkers of interest that exhibit absorption within the 8 – 13 μm region include propan-1-ol, propanoic and butanoic acids, and indole [2,55]. Additionally, longer wavelength regions are particularly useful in aromatic classification. Specifically, the 8 – 10 μm region is useful in determining the substituent groups on the benzene ring and the 11 – 15 μm region can also help determine group position on the ring, i.e. the ortho, meta, or para (*o*-, *m*-, or *p*-) isotopologue [56]. Shorter mid-IR bands caused by C-H and C=C vibrations are likely to be less helpful when trying to distinguish aromatics from other organic molecules.

2. Experimental setup

This section describes the experimental configuration of the spectrometer, which is shown in Fig. 1, and includes the laser system, detectors, and the construction of the hollow waveguide gas cell.

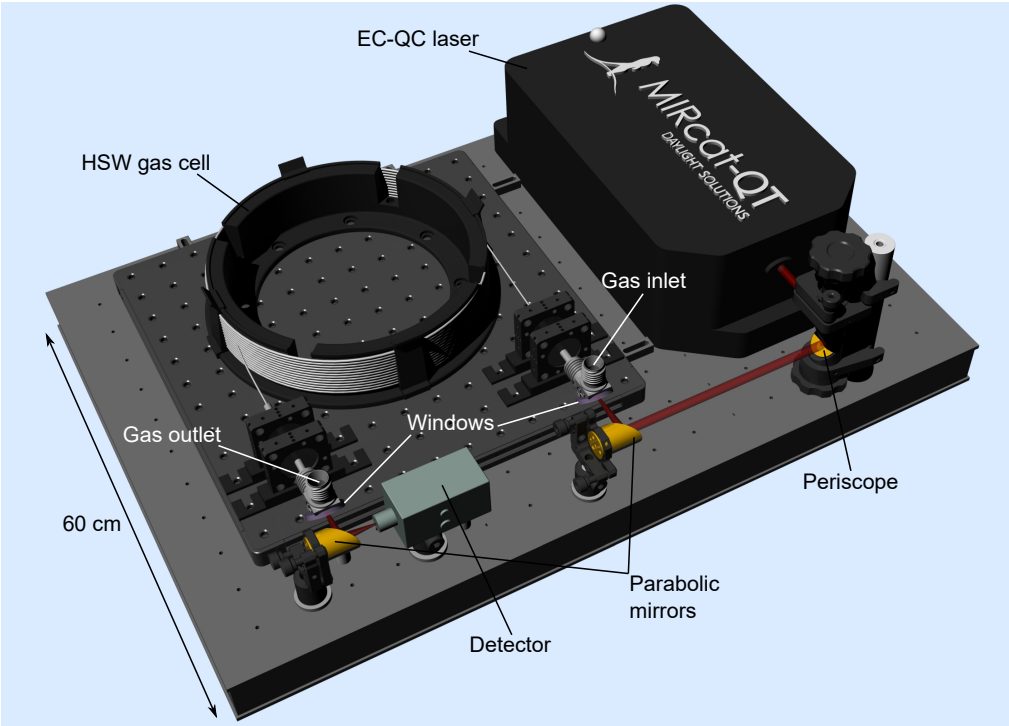


Fig. 1. A 3D diagram showing the layout of components comprising the spectrometer. (STEP files for optomechanics including the small breadboard, lens and mirror mounts, post holders, and periscope mount taken from https://www.thorlabs.com).

2.1. External-cavity quantum cascade laser system

The laser used in the spectrometer is a Daylight Solutions MIRcat-QT system that can support up to four QCL modules to provide a total tuning range from 3 – 13 μm (3,333 – 769 cm^{-1}). However, the system used here concentrates solely on the longer wavelength range and contains a single module (M2112-PX) which provides pulsed emission from 10 – 13 μm (1,000 – 769 cm^{-1}), with a maximum tuning rate of 5,000 cm s^{-1}. The wavelength accuracy of the laser which is quoted as <1 cm^{-1}, which is <~10 nm for our wavelength region. Tuning is achieved

Optics EXPRESS

by rotating a diffraction grating located within the laser housing. Without water cooling, the laser is limited to a duty cycle of 10% with a maximum pulsewidth of 1,000 ns and a maximum repetition rate of 100 kHz. Water cooling allows higher duty cycles, but at the cost of instrument portability, which is important for a point-of-care system. In our work, the laser was controlled using a USB interfaced laptop with custom developed software written in LabVIEW using the supplied software development kit. The software allows fixed static output wavelengths to be set as well as laser sweep ranges and their velocities in either cm^{-1} or μm. The beam exiting the laser was brought to a height of 5.5 cm where it was coupled into the gas cell using a 50.8 mm (2") focal length gold coated off-axis parabolic (OAP) mirror. Alignment of the beam was aided by a Thorlabs VRC6S infrared viewing card. Light exiting the gas cell was focused on to the detector using a 25.4 mm (1") OAP mirror.

2.2. Detection and digitization

The detector is a Vigo Photonics PCI-4TE-13, which is a photoconductive, optically immersed detector with four thermoelectric cooling stages and an active area of 1 mm^2. The detector is paired with a programmable preamplifier, which allows settings such as gain, bias voltage, and AC/DC coupling to be adjusted, and a PTCC-01 programmable thermoelectric cooler (TEC) controller. The detector has a peak detectivity at 11 μm with a D* value of approximately 3.8×10^{-9} and this drops to approximately 3.0×10^{-9} at 13 μm. The detector signal was digitized using an oscilloscope (NI PXIe-5170R housed in PXIe-1071 chassis). The oscilloscope was interfaced to a laptop using a high bandwidth Thunderbolt connection which allows up to 2.3 GB s^{-1} throughput. The oscilloscope has four channels each with 14 bit digital resolution and a maximum sampling rate of 250 MS s^{-1}.

2.3. Wavelength calibration using an optical spectrum analyser

Wavelength calibration was performed at a range of grating positions corresponding to set wavelength values at 100 nm increments across the full 10 – 13 μm range. This was done by directly coupling the QCL beam into a mid-IR optical spectrum analyser (OSA) (Thorlabs OSA207C) that was custom built to allow sensitivity up to 13 μm. The plot shown in Fig. 2(a) is a composite of 31 individual OSA measurements that have been made at each increment and where the signal magnitude has been normalized to unity. Whilst in subsequent measurements presented in this paper, the laser wavelength was swept, the laser wavelength was stepped for the calibration due to the measurement time required by the OSA. Each individual measurement took a minute or so to make with a total data collection time of around 30 minutes. The centre wavelength of each OSA measurement was determined using a peak localization method based on a short-term quadratic fit [57]. The measured wavelength plotted against the set wavelength is shown in Fig. 2(b) on the left y-axis (black trace). There was an offset of approximately 50 nm between the set wavelength and the measured wavelength which decreased with increasing wavelength. This difference is plotted in Fig. 2(b) on the right *y*-axis (red trace). This trend was repeatable when the measurements were made again twice subsequently, and this data was used to correct the wavelength values shown in the paper.

2.4. Hollow waveguide gas cell

Gas cells were constructed using hollow silica waveguides (Polymicro) that were 5 m in length with an internal bore diameter of 750 μm. This diameter, out of an available range that includes a minimum of 300 μm and a maximum 1,000 μm, offers a good compromise between mechanical flexibility and transmission. This is because larger diameter waveguides offer better light efficiency due to fewer reflections per unit length and smaller diameter waveguides are much more easily coiled. As the focused spot size is very small relative to the 750 μm aperture, coupling efficiency is high, however waveguide losses are significant. For this waveguide, the maximum

Optics EXPRESS

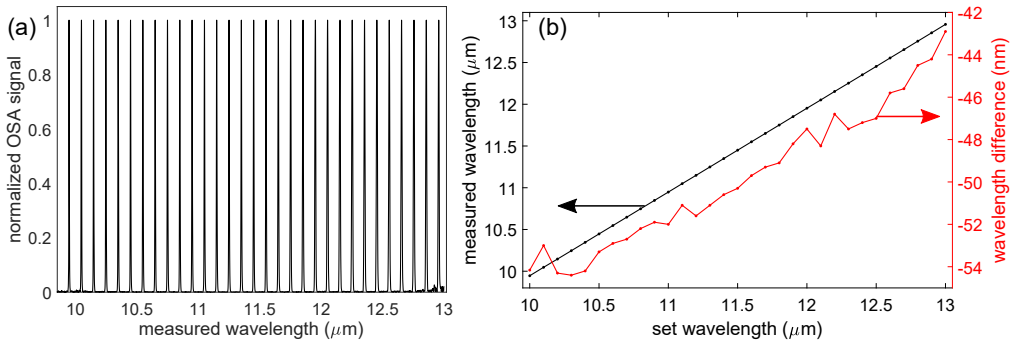


Fig. 2. Plots showing (a) normalized OSA measurements made at 100 nm increments across the 10 – 13 μm range of the tuneable laser, and (b) The variation in measured wavelength vs. the laser set wavelength (left *y*-axis) and the difference between them (right *y*-axis).

straight loss is 0.5 dBm^{-1} with a 1.0 dBm^{-1} bend loss per 360° in a 40 cm diameter loop [35]. Polycarbonate hollow waveguides [58] are an alternative to silica and due to their flexibility are particularly advantageous in the construction of larger gas cells with bore diameters up to ~6 mm. Silica however offers better flexibility for smaller bore diameters in the 300 – 1,000 μm range and lower surface roughness which results in lower loss at these diameters. The ends of the waveguide were inserted into sections of 1/8" (3.18 mm) outer diameter stainless-steel tubing on which Swagelok elbow fittings are attached [59]. The ends of the stainless-steel tubes opposite the fittings were sealed with a metal loaded epoxy. The fittings were modified so that a window could be embedded or affixed allowing gas and light to enter (or exit) the cell simultaneously. The windows chosen for use within the cell were made of chemical vapour deposition (CVD) diamond and were purchased from Crystran. Whilst CVD diamond is expensive, particularly for

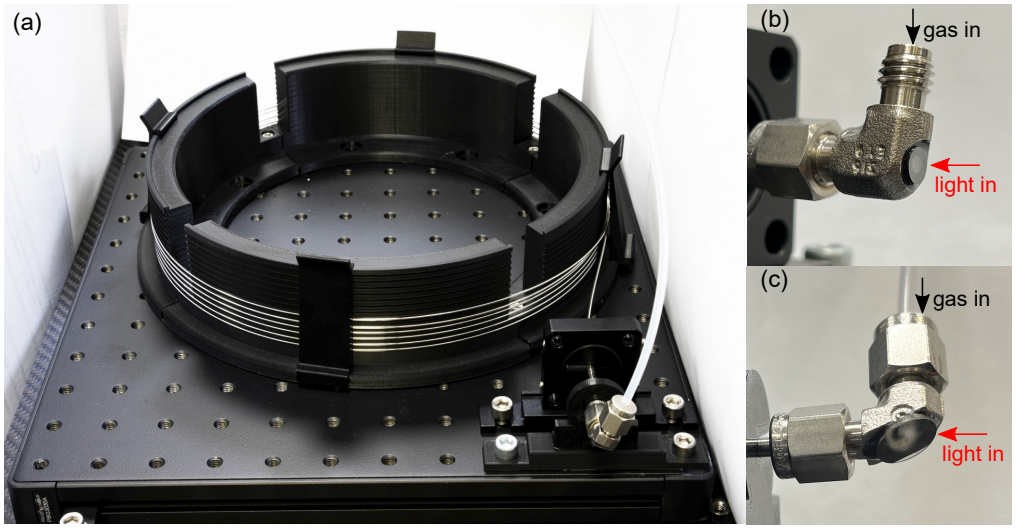


Fig. 3. Photographs showing the construction of the hollow waveguide gas cell: (a) shows the complete cell on the 24 cm diameter, custom designed 3D printed mount, (b) shows a modified Swagelok elbow fitting with a 5 mm diameter normally aligned CVD diamond window embedded, and (c) shows a modified fitting with a 10 mm diameter CVD diamond window aligned at the Brewster angle.

Optics EXPRESS

large windows, the smaller 5 mm diameter windows, used in one of the configurations here, are relatively affordable (~£350 GBP). CVD diamond was chosen because of its non-hygroscopic properties, robustness, and its flat transmission spectrum across the wavelength range of the laser of approximately 70%. The waveguide cell was mounted on an in-house designed, 3D printed that aids the mechanical stability of the cell and is shown in the photograph in Fig. 3(a).

Gas cells using two window configurations were built and tested: the first incorporated 5 mm diameter windows that were oriented orthogonally to the incoming beam (Fig. 3(b)), and the second used 10 mm diameter windows that were mounted at the Brewster angle (Fig. 3(c)). The Brewster angle for CVD diamond ranges from 67.14° to 67.18° [60] across the wavelength range of the laser and this variation in angle is significantly less than the accuracy with which the window can be mounted, which is estimated to be approximately ±5°. Alignment at the Brewster angle serves to reduce etalon fringing within the window due to suppression of the P-polarized reflection. The degree of suppression is a relatively weak function of angle, at angles close to the Brewster angle, and obvious suppression could still be obtained even though the mounting accuracy was low.

3. Spectrum acquisition

Spectrum acquisition was performed by first setting the laser to sweep continuously from low wavelength to high wavelength. Although bi-directional sweeping is an option with the MIRcat system, single-direction sweeping was solely used here. The oscilloscope was triggered by the rising edge of a TTL signal that corresponds to the tuning state of the laser, with a HI signal (+5V) emitted when the sweep initiates and which continues until the sweep terminates. Triggering in this way ensures that pulse trains acquired on consecutive sweeps are in the same spectral position. This allows the averaging of sequences of spectra which improves the signal-to-noise ratio.

The acquired pulse trains were processed to generate the raw spectra. A binary threshold filter was first applied to determine the locations of the off-pulse and on-pulse data. This method was found to have a shorter execution time than other methods tried (such as differentiation of the pulse train), which is important for providing real-time processing. The mean value of the central portion of the on-pulse data was calculated for each individual pulse and a section of the off-pulse data of equal length was also averaged and subsequently subtracted to remove the local background. Figure 4(a) shows a section of a typical pulse train acquired during a laser sweep and

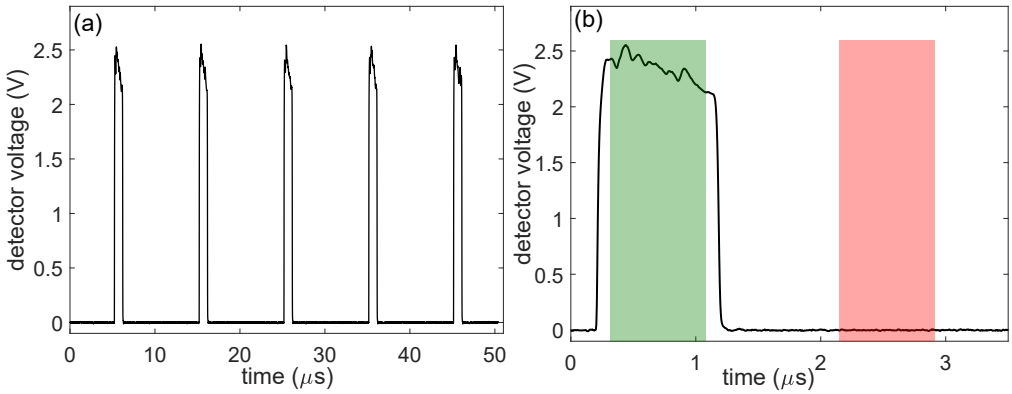


Fig. 4. (a) A plot showing a section of a typical pulse train recorded during a laser sweep. (b) A single pulse with green and red highlighted blocks indicating the approximate region of the on-pulse and off-pulse signal that is averaged and differenced to build up the spectrum.

Optics EXPRESS

Fig. 4(b) shows the regions of the averaged data highlighted for an individual pulse. Spectra were then constructed from the averaged pulse data in a process known as the inter-pulse technique [61]. This is opposed to the intra-pulse technique in which the spectral tuning occurs across individual laser pulses. To ensure that the processing is carried out in real-time, this averaging procedure needs to be applied to the entire pulse-train within the time that the laser sweeps and resets to its start point prior to the next sweep. Therefore, a careful choice of digitization rate and sweep velocity was made ensuring, additionally, that individual pulse trains could be stored on the onboard memory of the oscilloscope (0.75 GB). Some of the sweep velocities used in this work for sweeps covering the range from 10.2 μm and 11.6 μm and the digitization rates used are provided in Table 2.

Table 2. Digitization rates used for different sweep velocities covering the range from 10.2 – 11.6 μm.

Sweep velocity (μm s^{-1})	Digitization rate (MS s^{-1})
1	6.25
2	12.5
5[a]	25
10[a]	50
20	125
50[a]	250

[a](Sweep velocities used in this paper).

Raw spectra were generated from the processed pulsed trains and examples are shown in Fig. 5(a) for gas cells with the two different diamond window configurations shown in Fig. 3(b) and Fig. 3(c). These spectra were acquired with no active gas flow through the cell. The structure seen is the result of the combination of etalon fringing within the windows and inter-modal interference occurring within the hollow waveguide. The upper trace (red) was acquired using the orthogonally aligned, planar windows, and the lower trace (black) using the Brewster aligned windows. The result of the Brewster aligned windows is the suppression of fringes at particular frequencies, which can be illustrated using Fourier analysis. The signals from the two gas cells were acquired with the laser scanning in wavelength however, to remove the frequency chirp from the fringe patterns and thus sharpen the Fourier peaks, the data was interpolated from the linear wavelength scale to a non-linear wavenumber scale. The fast Fourier transform (FFT) of the signals associated with the planar window and Brewster window configurations are shown in red and black in Fig. 5(b) respectively. The prominent frequency at 0.48 cm seen in the planar window configuration is completely suppressed in the Brewster window configuration. This frequency is associated with reflections within the input window of the cell. The smaller peak at 0.96 cm that is also suppressed is due to multiple reflections within this window. The other prominent frequency at 0.62 cm is caused by reflections within the output window and this is not suppressed by the Brewster aligned window due to depolarization of light propagating through the hollow waveguide. Any mechanical or environmental disturbance of the gas cell can cause changes in these frequencies which leads to the introduction of fringes into the referenced measurement. Removal of some of these frequencies by using Brewster aligned windows results in fewer etalons that can potentially affect the absorption measurement yielding a more stable system. This is believed to be the first demonstration of signal improvement using Brewster aligned windows within a hollow silica waveguide gas cell. Previously we used them [36] within a spectrometer in which there were no interference fringe issues and so did not see any signal improvement at that time.

Optics EXPRESS

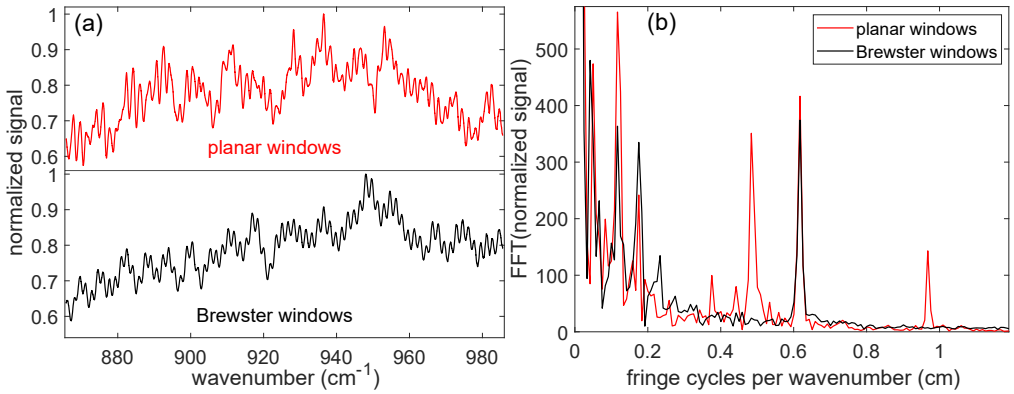


Fig. 5. (a) Raw spectra acquired through hollow waveguide gas cells with planar diamond windows (upper-red) and Brewster aligned diamond windows (lower-black). (b) The FFTs of the signals in (a) with frequencies at 0.48 cm and 0.96 cm associated with the input windows and a frequency at 0.62 cm associated with the output windows.

4. Propane measurements

To test the spectrometer, a gas supply system was set up consisting of a network of mass flow controllers (MFCs) (Brooks GF040CXX) interfaced to a controller (Brooks Instrument 0254). The MFCs each have an accuracy of 1% of the reading. An MFC with a flow range from 0 – 1,000 sccm (standard cubic centilitres per minute) was connected to a cylinder of zero-grade, hydrocarbon-free air, with a similar MFC connected to a cylinder containing 1,000 ppm propane in air. By changing the ratio of flows through the two MFCs, the concentration could be varied in the range 0 – 1,000 ppm. Propane was chosen as a test gas due to it being easy to handle and safe at this concentration, as well as its broad absorption within the spectral range of the instrument, which has similar characteristics to many other VOCs. Propane absorption within the instrument's spectral range is dominated by the ν_{21} band which spans the region from 10.55 – 11.6 μm (948 – 896 cm^{-1}) [41]. Setting the laser to sweep between 10.2 μm and 11.6 μm captures the entire band, plus a region of spectrally sparse baseline at lower wavelengths. At longer wavelengths (>11.2 μm) there is also some contribution from the ν_8 band.

The laser was set to sweep at a rate of 5 μm s^{-1} which, including the downtime between each sweep, resulted in a spectrum acquisition rate of ~0.75 Hz. A series of raw spectra was then recorded whilst a flow of clean air passed through the cell. The spectra were averaged, and the result was saved in memory to be used as a reference spectrum. The gas passing through the cell was then switched to propane and normalized absorption spectra were generated based on the Beer-Lambert law [5]

$$\frac{V(\lambda)}{V_0(\lambda)} = e^{-\alpha(\lambda)l} \tag{1}$$

where $V_0(\lambda)$ is the detector signal corresponding to the reference spectrum, $V(\lambda)$ is the signal corresponding to subsequently acquired spectra, $\alpha(\lambda)$ is the concentration dependent absorption coefficient (in cm^{-1}) and l is the pathlength (in cm). As the pathlength of the HSW gas cell is known (5 m), the absorbance can be presented in dimensionless absorbance units (au). Figure 6(a) shows an absorption spectrum acquired in the presence of 1,000 ppm propane calculated using Eq. (1). As there is a significant level of high frequency noise in the absorption spectrum it was processed using a Gaussian weighted convolution filter (Fig. 6(b)). This is fast operation that can be performed in real-time on each individual spectrum as it is acquired. Spectra were collected over a period of ~2 minutes and were cumulatively averaged to reduce the noise. Some spectra were affected by interference fringing introduced by environmental disturbances, and these were

Optics EXPRESS

selectively rejected from the averaging process. Spectra that were affected significantly were determined by comparing the baseline to the reference. This was done by calculating the mean difference in the baseline of measurements made relative to measurements made in air, with spectra having greater differences being rejected. Approximately 20% of spectra were rejected in this manner. The resulting spectrum obtained after cumulative averaging is shown in Fig. 6(c). This averaging was performed as a post-process after the spectra were acquired. Finally, the spectrum was processed with a Fourier bandpass filter to provide further suppression of noise, as shown in Fig. 6(d). The measurements were made in an optical laboratory with ambient temperature and pressure of 295 K and 101.8 kPa respectively.

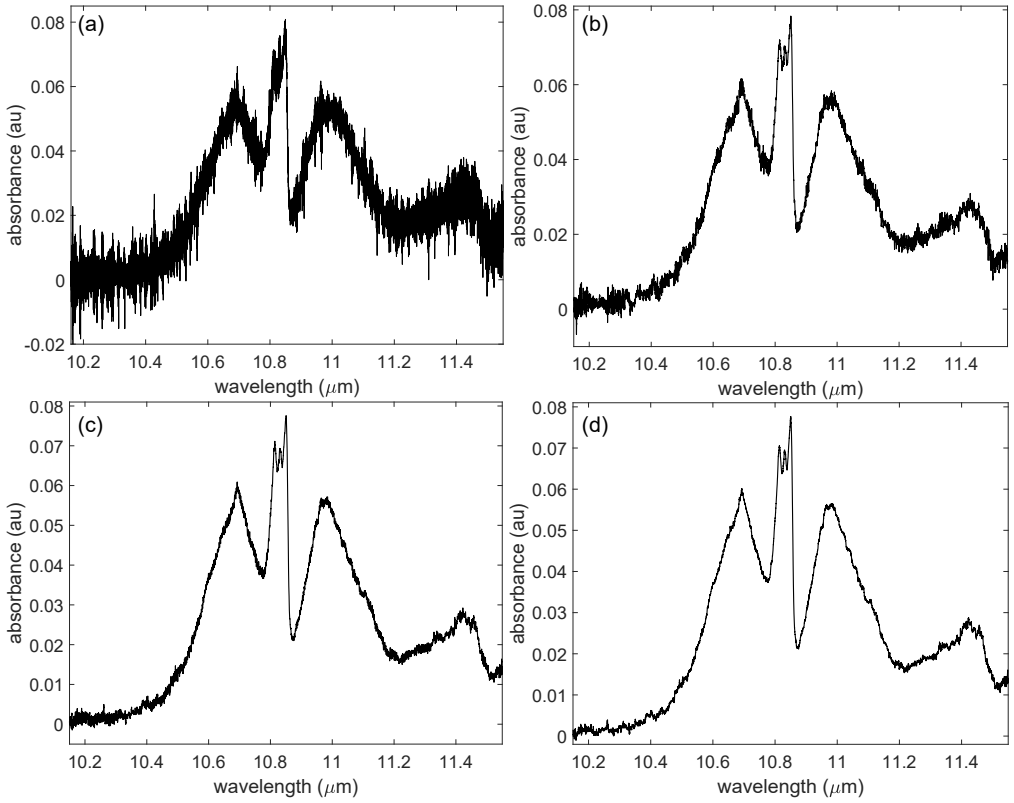


Fig. 6. The processing sequence for normalized absorption spectra acquired in the presence of 1,000 ppm propane: (a) a spectrum obtained using the Beer-Lambert law Eq. (1) on signals obtained with air and propane. (b) after smoothing with a convolution filter. (c) after cumulative averaging, including rejection via baseline comparison, of measurements made over a ~2 minute period. (d) after processing with a Fourier filter.

The measured spectrum was compared to data from an FTIR scan that was made by Sung *et al.* in the 7 – 15 μm region to support spectroscopic findings in the atmosphere of Titan and other planets [62]. The scan data has been made publicly available on the HITRAN database [63]. Several FTIR scans over this region are available on the database made at a range of temperatures and pressures with the one shown here having been obtained at 297.0 K and 740.2 Torr (98.7 kPa) with a spectral resolution of 0.0033 cm^{-1}, which mostly closely matches the conditions in which our QCL spectrometer was used. Figure 7 shows an absorption spectrum overlaid on the FTIR scan over the same spectral range and the two traces show good agreement.

Optics EXPRESS

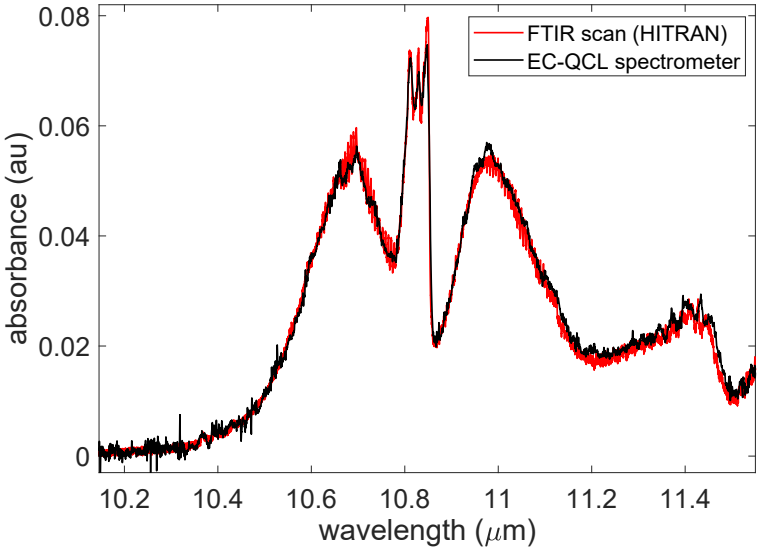


Fig. 7. A plot showing the absorption spectrum of propane in the 10.2 – 11.6 μm region acquired using the external cavity QCL spectrometer. For comparison, the spectrum acquired using an FTIR spectrometer, which is used on the HITRAN database, is also shown [62,63]. The EC-QCL trace (in black) has been processed to the same extent as that in Fig. 6(d).

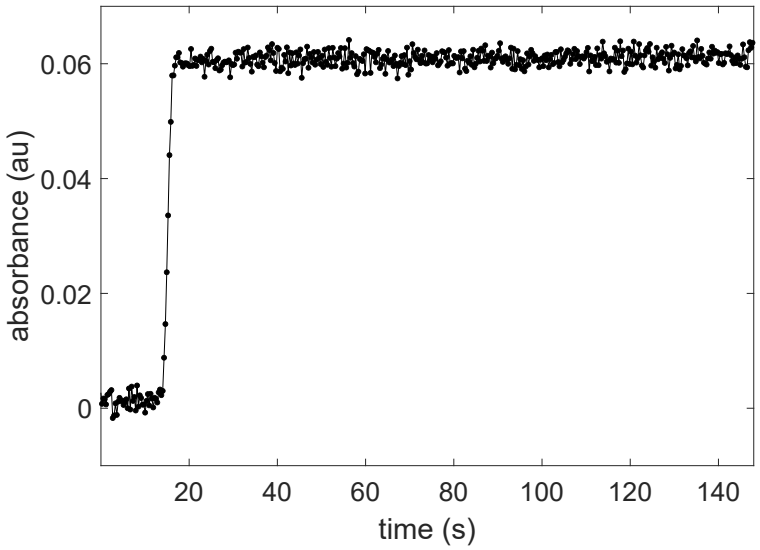


Fig. 8. The variation in absorbance over the course of a measurement. Data was acquired at an increased sweep rate of 50 μm s^{-1} allowing a spectrum acquisition rate of ~3 Hz, demonstrating the response of the cell. The $t_{90} - t_{10}$ rise time is 1.8 s.

The variation in absorbance over the duration of a typical measurement is shown in Fig. 8. In this example, the sweep velocity was set to 50 μm s^{-1}, which is close to the maximum sweep rate of the laser. This enabled an increased spectrum acquisition rate at the cost of greater noise and reduced spectral resolution. An acquisition rate of ~3 Hz was achieved at this sweep velocity, and this helps to illustrate the cell response. Absorption values were evaluated for each individual spectrum by averaging the central absorption feature (from ~10.78 – 10.86 μm) and subtracting

Optics EXPRESS

the mean background level (taken from ~10.18 – 10.26 μm). Each individual spectrum was processed with a convolution filter and were therefore similar to the one in Fig. 6(b). The t_{90} – t_{10} rise time calculated from this data is 1.8 s. A total flow rate of 700 sccm was maintained throughout which consisted solely of air until ~15 s, and after was switched to 1,000 ppm propane. The pressure measured at the inlet of the gas cell was 2.1 ± 0.1 bar.

The response linearity was evaluated by using the MFC network to gradually dilute the flow of propane to the cell whilst the molecular absorption was measured. An additional MFC with output flow rates covering the range from 10 – 100 sccm was used to generate lower concentration gas mixtures. The gas mixtures generated had approximate concentrations ranging from 20 – 100 ppm in steps of 20 ppm and 100 – 1,000 ppm in steps of 100 ppm which were directed to the cell. At each concentration level, spectra were acquired for approximately 2 minutes and the absorbance calculated from each spectrum was averaged. Absorption values for each spectrum were evaluated in the same manner as described previously. The resulting absorbance measurements are shown in Fig. 9, where the error bars represent the standard deviation of measurements made at each concentration and the straight line shows a linear fit to the data. The inset shows the absorption measurements made at lower concentrations more clearly.

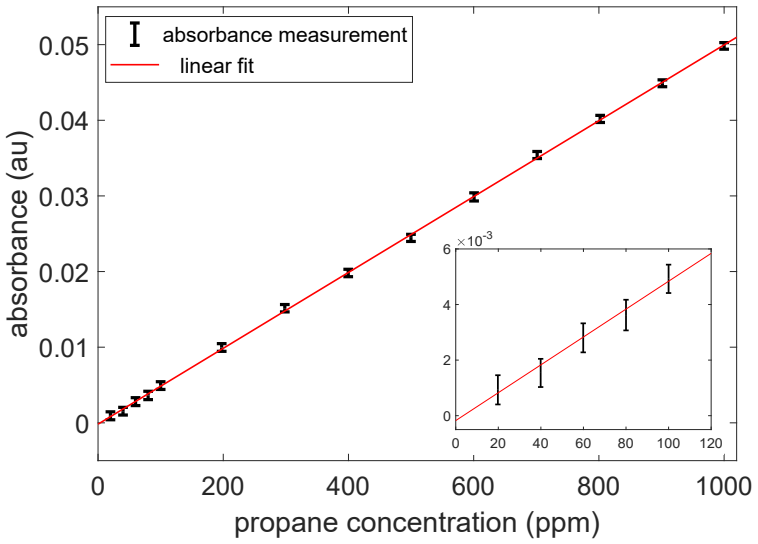


Fig. 9. Absorbance measurements made at a range of propane concentration levels obtained by diluting the flow of propane at 1,000 ppm with zero-grade air. Each point is the mean of values recorded over ~2 mins and the error bars are derived from the standard deviation of each measurement step. The linear fit shown has R^2 = 0.9998. The inset shows the measurements made with the lower flow MFC at concentrations ranging from 20 – 100 ppm more clearly.

The Allan-Werle deviation of a time-series of absorption data can provide important information on the performance of a spectrometer [64]. Figure 10(a) shows an absorption time-series recorded over a period of almost 100 minutes with a mean interval of 0.63 s. The absorption values were calculated in the same way as the previous measurements. The Allan deviation calculated from this data is shown in Fig. 10(b). The curve shows that averaging can improve the limit of detection until the minimum is reached, after which drift dominates. The minimum here is at approximately 75 s and corresponds to a minimum detectable absorbance of ~3.5×10^{-5}. This value is representative of the timeframe under which the spectrometer would be used for the intended VOC measurements, including a prior zero measurement being made, as a measurement

Optics EXPRESS

rate of every few minutes is perfectly adequate. This minimum detectable absorbance corresponds to a limit of detection of ~800 ppb for the propane absorption discussed here.

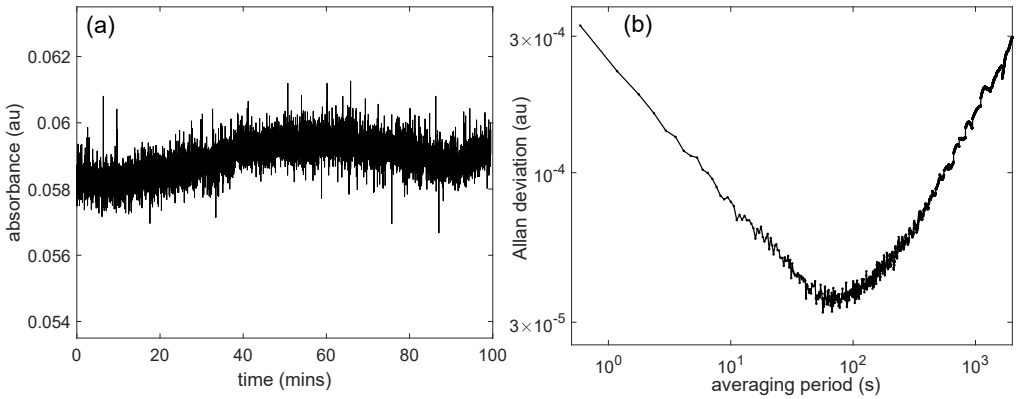


Fig. 10. (a) Time series of absorption data recorded over ~100 mins. (b) Allan deviation of that absorption data.

5. Discussion and conclusion

This paper has described the development of a pulsed external-cavity QCL spectrometer built in conjunction with a HSW gas cell. The laser operates in pulsed mode with spectra generated using the inter-pulse technique with fast digitization of swept pulse trains. Hollow silica waveguides were used to construct low-volume, fast-response gas cells with gas/light couplers made using modified gas compression fittings. Gas cells were made using CVD diamond windows in planar and Brewster aligned configurations, with the Brewster aligned windows providing suppression of the fringes associated with reflections within the input window. Propane is a convenient test gas and its mid- to long-wave infrared spectrum has been well studied. The ν_{21} band, which is measured here, is a relatively weak absorption but has generated interest due to its detection in the atmosphere of Titan by the Cassini probe. The Allan deviation of a time-series of absorption data indicates a minimum detectable absorbance of 3.5×10^{-5} after an averaging period of 75 s. The system is currently limited by the scanning rate as there would be better rejection of vibrations with much faster spectral scans made up to ~1 kHz.

The instrument has been developed to allow quantification of volatile biomarkers and one that is of particular interest is *p*-cresol, a compound observed in elevated levels in hospital patients with *Clostridium-difficile* infection. Infrared absorption cross-sections were recorded using an FTIR spectrometer in a publication by Etzkorn *et al.* [54]. A targetable absorption is available that is centred at ~12.2 μm (820 cm^{-1}). The absolute and integrated cross-sections for this absorption are given in Table 3. For comparison, the values for the propane ν_{21} absorption are also provided, acquired from data taken from the HITRAN database. The propane absorption is approximately 50 times weaker, both in terms of absolute and integrated cross-section, than the *p*-cresol absorption that we intend to target. Based on the minimum detectable absorbance of the spectrometer, a limit of detection for *p*-cresol in the 10s of ppb range should be achievable, which is at the level required to be valuable in a clinical environment.

The spectrometer is suitable for measurement of VOCs and can potentially be used to monitor VOC concentrations in the headspace gas of patient samples within hospital settings. The use of a long-wave infrared spectrometer is important for identifying aromatic VOCs, which are particularly significant. Such applications typically provide small sample volumes for analysis, requiring the use of gas cells with large pathlength-to-volume ratio. In addition, the instrument's

Optics EXPRESS

Table 3. Comparison of cross-sections of targeted absorptions of propane and *p*-cresol taken from the literature. (wl = wavelength, wn = wavenumber).

	Absolute cross section		Integrated cross section		Ref
	wl(wn) μm(cm^{-1})	10^{-21} cm^2 $molecule^{-1}$	Range μm(cm^{-1})	10^{-19} cm $molecule^{-1}$	
propane ν_{21}	10.85 (922)	6.52	10.55 – 11.16 (948 – 896)	1.79[a]	[62]
p-cresol	12.20 (820)	355 ± 7.0	11.57 – 12.94 (864 – 773)	91.5	[54]

[a]Value acquired by numerically integrating FTIR data taken from HITRAN database.

optimum averaging period of 75 s is compatible with obtaining a time-to-result within a few minutes. This has the potential to lead to point-of-care instrumentation facilitating the diagnosis of gastrointestinal conditions in a much faster timeframe than could be achieved when relying on GCMS analysis in external laboratories.

Funding. Engineering and Physical Sciences Research Council (EP/P015603/1).

Acknowledgments. The authors would like to acknowledge support from the Engineering and Physical Sciences Research Council via grant EP/P015603/1.

Disclosures. The authors declare no conflicts of interest.

Data availability. The underlying data can be accessed through the Cranfield University data repository at [65].

References

1. D. K. Trivedi, E. Sinclair, Y. Xu, *et al.*, "Discovery of volatile biomarkers of Parkinson's disease from sebum," ACS Cent. Sci. **5**(4), 599–606 (2019).
2. C. Walton, D. P. Fowler, C. Turner, *et al.*, "Analysis of volatile organic compounds of bacterial origin in chronic gastrointestinal disease," Inflamm. Bowel Dis. **19**(10), 2069–2078 (2013).
3. W. Carroll, W. Lenney, T. Wang, *et al.*, "Detection of volatile compounds emitted by *pseudomonas aeruginosa* using selected ion flow tube mass spectrometry," Pediatr. Pulm. **39**(5), 452–456 (2005).
4. H. I. Schiff, G. I. Mackay, and J. Bechara, "The use of tuneable diode laser absorption spectroscopy for atmospheric measurements," Res. Chem. Intermed. **20**(3-5), 525–556 (1994).
5. J. Hodgkinson and R. P. Tatam, "Optical gas sensing: a review," Meas. Sci. Technol. **24**(1), 012004 (2013).
6. J. B. McManus, M. S. Zahniser, D. D. Nelson, *et al.*, "Application of quantum cascade lasers to high-precision atmospheric trace gas measurements," Opt. Eng. **49**(11), 111124 (2010).
7. M. R. McCurdy, Y. Bakhirkin, G. Wysocki, *et al.*, "Recent advances of laser-spectroscopy-based techniques for applications in breath analysis," J. Breath Res. **1**(1), 014001 (2007).
8. A. Schwaighofer, M. Brandstetter, and B. Lendl, "Quantum cascade lasers (QCLs) in biomedical spectroscopy," Chem. Soc. Rev. **46**(19), 5903–5924 (2017).
9. E. L. Normand, I. Howieson, M. McColloch, *et al.*, "Quantum cascade laser (QCL) based sensor for the detection of explosive compounds," Proc. SPIE **6402**, 64020G (2006).
10. E. L. Normand, R. J. Stokes, K. Hay, *et al.*, "Advances in quantum cascade lasers for security and crime-fighting," Proc. SPIE **7838**, 78380A (2010).
11. T. Iseki, H. Tai, and K. Kimura, "A portable remote methane sensor using a tunable diode laser," Meas. Sci. Technol. **11**(6), 594–602 (2000).
12. Z. Du, S. Zhang, J. Li, *et al.*, "Mid-infrared tunable laser-based broadband fingerprint absorption spectroscopy for trace gas sensing: a review," Appl. Sci. **9**(2), 338 (2019).
13. J. Faist, F. Capasso, D. L. Sivco, *et al.*, "Quantum cascade laser," Science **264**(5158), 553–556 (1994).
14. J. R. Meyer, W. W. Bewley, C. C. Canedy, *et al.*, "The interband cascade laser," Photonics **7**(3), 75 (2020).
15. F. Capasso, "High-performance midinfrared quantum cascade lasers," Opt. Eng. **49**(11), 111102 (2010).
16. W. Ju, C. Lu, Y. Zhang, *et al.*, "Characteristic wavelength selection of volatile organic compounds infrared spectra based on improved interval partial least squares," J. Innov. Opt. Heal. Sci. **12**(02), 1950005 (2019).
17. Y. Ma, K. Ding, L. Wei, *et al.*, "Research on mid-infrared external cavity quantum cascade lasers and applications," Crystals **12**(11), 1564 (2022).
18. M. R. Alcaráz, A. Schwaighofer, C. Kristament, *et al.*, "External-cavity quantum cascade laser spectroscopy for mid-ir transmission measurements of proteins in aqueous solution," Anal. Chem. **87**(13), 6980–6987 (2015).
19. A. Schwaighofer, M. Montemurro, S. Freitag, *et al.*, "Beyond fourier transform infrared spectroscopy: External cavity quantum cascade laser-based mid-infrared transmission spectroscopy of proteins in the amide I and amide II region," Anal. Chem. **90**(11), 7072–7079 (2018).

Optics EXPRESS

20. C. J. Breshike, C. A. Kendziora, R. Furstenburg, *et al.*, "Methodology for using active infrared spectroscopy in standoff detection of trace explosives," Proc. SPIE **10183**, 1018302 (2017).
21. X. Liu, I. Chae, N. Miriyala, *et al.*, "Broadband mid-infrared stand-off reflection–absorption spectroscopy using a pulsed external cavity quantum cascade laser," Appl. Spectrosc. **71**(7), 1494–1505 (2017).
22. T. K. Boyson, D. R. Rittman, T. G. Spence, *et al.*, "Pulsed quantum cascade laser based hypertemporal real-time headspace measurements," Opt. Express **22**(9), 10519–10534 (2014).
23. N. Liu, S. Zhou, L. Zheng, *et al.*, "Standoff detection of VOCs using external cavity quantum cascade laser spectroscopy," Laser Phys. Lett. **15**(8), 085701 (2018).
24. J. Sun, J. Ding, N. Liu, *et al.*, "Detection of multiple chemicals based on external cavity quantum cascade laser spectroscopy," Spectrochim. Acta A **191**, 532–538 (2018).
25. J. M. Kriesel, C. N. Makarem, M. C. Phillips, *et al.*, "Versatile, ultra-low sample volume gas analyzer using a rapid, broad-tuning ECQCL and a hollow fiber gas cell," Proc. SPIE **10210**, 1021003 (2017).
26. B. E. Brumfield, M. S. Taubman, and M. C. Phillips, "Rapid and sensitive quantification of isotopic mixtures using a rapidly-swept external cavity quantum cascade laser," Photonics **3**(2), 33 (2016).
27. R. Brechbühler, M. Selakovic, P. Scheidegger, *et al.*, "Rapid detection of volatile organic compounds by switch-scan tuning of Vernier quantum-cascade lasers," Anal. Chem. **95**(5), 2857–2864 (2023).
28. M. Nikodem, "Laser-based trace gas detection inside hollow fibers: a review," Materials **13**(18), 3983 (2020).
29. F. Benabid, F. Couny, J. C. Knight, *et al.*, "Compact, stable and efficient all-fibre gas cells using hollow-core photonic crystal fibres," Nature **434**(7032), 488–491 (2005).
30. J. A. Nwaboh, J. Hald, J. K. Lyngsø, *et al.*, "Measurements of CO_2 in a multipass cell and in a hollow-core photonic bandgap fiber at 2 µm," Appl. Phys. B **110**(2), 187–194 (2013).
31. A. Wilk, J. C. Carter, M. Chrisp, *et al.*, "Substrate-integrated hollow waveguides: A new level of integration in mid-infrared gas sensing," Anal. Chem. **85**(23), 11205–11210 (2013).
32. J. A. Harrington, "A review of ir transmitting hollow waveguides," Fiber Integr. Opt. **19**(3), 211–227 (2000).
33. T. Wu, W. Kong, M. Wang, *et al.*, "Compact hollow waveguide mid-infrared gas sensor for simultaneous measurements of ambient CO_2 and water vapor," J. Lightwave Technol. **38**(16), 4580–4587 (2020).
34. P. Patimisco, V. Spagnolo, M. S. Vitiello, *et al.*, "Coupling external cavity mid-IR quantum cascade lasers with low loss hollow metallic/dielectric waveguides," Appl. Phys. B **108**(2), 255–260 (2012).
35. D. Francis, J. Hodgkinson, B. Livingstone, *et al.*, "Quantum cascade laser light propagation through hollow silica waveguides," Appl. Phys. B **119**(1), 75–86 (2015).
36. D. Francis, J. Hodgkinson, B. Livingstone, *et al.*, "Low-volume, fast response-time hollow silica waveguide gas cells for mid-ir spectroscopy," Appl. Opt. **55**(25), 6797–6806 (2016).
37. P. Patimisco, V. Spagnolo, M. S. Vitiello, *et al.*, "Low-loss hollow waveguide fibers for mid-infrared quantum cascade laser applications," Sensors **13**(1), 1329–1340 (2013).
38. V. Spagnolo, P. Patimisco, S. Borri, *et al.*, "Mid-infrared fiber-coupled QCL-QEPAS sensor," Appl. Phys. B **112**(1), 25–33 (2013).
39. W. Chen, S. Qiao, Z. Lang, *et al.*, "Hollow-waveguide-based light induced thermoelastic spectroscopy sensing," Opt. Lett. **48**(15), 3989–3992 (2023).
40. W. Chen, S. Qiao, Y. He, *et al.*, "Mid-infrared all-fiber light-induced thermoelastic spectroscopy sensor based on hollow-core anti-resonant fiber," Photoacoustics **36**, 100594 (2024).
41. A. Perrin, F. Kwabia-Tchana, J. M. Flaud, *et al.*, "First high resolution analysis of the ν_{21} band of propane $CH_3CH_2CH_3$ at 921.382 cm^{-1}: Evidence of large amplitude tunneling effects," J. Mol. Spectrosc. **315**, 55–62 (2015).
42. J. Haas, E. V. Catalán, P. Piron, *et al.*, "Infrared spectroscopy based on broadly tunable quantum cascade lasers and polycrystalline diamond waveguides," Analyst **143**(21), 5112–5119 (2018).
43. R. Heinrich, A. Popescu, A. Hangauer, *et al.*, "High performance direct absorption spectroscopy of pure and binary mixture hydrocarbon gases in the 6–11 µm range," Appl. Phys. B **123**(8), 223 (2017).
44. A. Karpf and G. N. Rao, "Absorption and wavelength modulation spectroscopy of NO_2 using a tunable, external cavity continuous wave quantum cascade laser," Appl. Opt. **48**(2), 408–413 (2009).
45. R. M. Spearrin, S. Li, D. F. Davidson, *et al.*, "High-temperature *iso*-butene absorption diagnostic for shock tube kinetics using a pulsed quantum cascade laser near 11.3 µm," P. Combust. Inc. **35**(3), 3645–3651 (2015).
46. C. Young, S.-S. Kim, Y. Luzinova, *et al.*, "External cavity widely tunable quantum cascade laser based hollow waveguide gas sensors for multianalyte detection," Sensor. Actuat. B-Chem. **140**(1), 24–28 (2009).
47. H. Yi, T. Wu, A. Lauraguais, *et al.*, "High-accuracy and high-sensitivity spectroscopic measurement of dinitrogen pentoxide (N_2O_5) in an atmospheric simulation chamber using a quantum cascade laser," Analyst **142**(24), 4638–4646 (2017).
48. M. C. Phillips, M. S. Taubman, B. E. Bernacki, *et al.*, "Real-time trace gas sensing of fluorocarbons using a swept-wavelength external cavity quantum cascade laser," Analyst **139**(9), 2047–2056 (2014).
49. A. Reyes-Reyes, Z. Hou, E. van Mastrigt, *et al.*, "Multicomponent gas analysis using broadband quantum cascade laser spectroscopy," Opt. Express **22**(15), 18299–18309 (2014).
50. A. Reyes-Reyes, R. C. Horsten, H. P. Urbach, *et al.*, "Study of the exhaled acetone in type 1 diabetes using quantum cascade laser spectroscopy," Anal. Chem. **87**(1), 507–512 (2015).
51. C. L. Strand, Y. Ding, S. E. Johnson, *et al.*, "Measurement of the mid-infrared absorption spectra of ethylene (C_2H_4) and other molecules at high temperatures and pressures," J. Quant. Spectrosc. Ra. **222-223**, 122–129 (2019).

Optics EXPRESS

52. I. Sydoryk, A. Lim, W. Jäger, *et al.*, "Detection of benzene and toluene gases using a midinfrared continuous-wave external cavity quantum cascade laser at atmospheric pressure," Appl. Opt. **49**(6), 945–949 (2010).
53. M. Patel, D. Fowler, J. Sizer, *et al.*, "Faecal volatile biomarkers of *Clostridium difficile* infection," PLoS One **14**(4), e0215256 (2019).
54. T. Etzkorn, B. Klotz, S. Sørensen, *et al.*, "Gas-phase absorption cross sections of 24 monocyclic aromatic hydrocarbons in the uv and ir spectral ranges," Atmos. Environ. **33**(4), 525–540 (1999).
55. NIST, "NIST chemistry webbook," Https://webbook.nist.gov/chemistry/ (accessed 21/02/24).
56. C. J. Pouchert, "The aldrich library of infrared spectra. ed 3," (1981). Aldrich Chemical Company (Milwaukee, WN, USA).
57. "Peak detection using LabVIEW and Measurement Studio," ni.com (2020) [accessed 12/04/2023], https://www.ni.com/en-gb/support/documentation/supplemental/06/peak-detection-using-labview-and-measurement-studio.html.
58. R. George and J. A. Harrington, "Infrared transmissive, hollow plastic waveguides with inner Ag-AgI coatings," Appl. Opt. **44**(30), 6449–6455 (2005).
59. D. Francis, E. J. Hodgkinson, and R. P. Tatam, "Hollow fibre waveguide gas cells," (2016). International patent WO2016/181100 A1.
60. M. N. Polyanskiy, "Refractive index database," https://refractiveindex.info (accessed 12/04/2023).
61. J. Manne, W. Jäger, and J. Tulip, "Sensitive detection of ammonia and ethylene with a pulsed quantum cascade laser using intra and interpulse spectroscopic techniques," Appl. Phys. B **94**(2), 337–344 (2009).
62. K. Sung, G. C. Toon, A. W. Mantz, *et al.*, "Ft-ir measurements of cold C_3H_8 cross sections at 7–15 μm for titan atmosphere," Icarus **226**(2), 1499–1513 (2013).
63. I. E. Gordon, L. S. Rothman, R. J. Hargreaves, *et al.*, "The HITRAN2020 molecular spectroscopic database," J. Quant. Spectrosc. Radiat. Transf. **277**, 107949 (2022).
64. P. Werle, R. Mücke, and F. Slemr, "The limits of signal averaging in atmospheric trace-gas monitoring by tunable diode-laser absorption spectroscopy (TDLAS)," Appl. Phys. B **57**(2), 131–139 (1993).
65. D. Francis, J. Hodgkinson, and R. P. Tatum, "Long-wave infrared pulsed external-cavity QCL spectrometer using a hollow waveguide gas cell," *Cranfield University data repository*, (2023).

62.255.49.186 {ts '2024-05-14 07:43:00'}



https://dspace.org/

Long-wave infrared pulsed external-cavity QCL spectrometer using a hollow waveguide gas cell

Francis, Daniel; Hodgkinson, Jane; Tatam, Ralph P.

2024-05-06
Optica Publishing Group
http://doi.org/10.1364/oe.521695
Francis D, Hodgkinson J, Tatam RP. (2024) Long-wave infrared pulsed external-cavity QCL spectrometer using a hollow waveguide gas cell. Optics Express, Volume 32, Issue 10, May 2024, pp.18399-18414

Downloaded from a DSpace repository. https://dspace.org/